Coexistence of singlet and ordered $S = \frac{1}{2}$ moments in the ground state of the triclinic quantum magnet $CuMoO_4$

S. Haravifard,[1,*] K. Fritsch,[1] T. Asano,[1,2] J. P. Clancy,[1] Z. Yamani,[3] G. Ehlers,[4] T. Nishimura,[2] Y. Inagaki,[5] T. Kawae,[5] I. Swainson,[3] and B. D. Gaulin[1,6,7]

[1]*Department of Physics and Astronomy, McMaster University, Hamilton, Ontario, Canada L8S 4M1*

[2]*Department of Physics, Kyushu University, Fukuoka 812-8581, Japan*

[3]*Canadian Neutron Beam Centre, NRC, Chalk River Laboratories, Chalk River, Ontario, Canada K0J 1J0*

[4]*Neutron Scattering Science Division, Oak Ridge National Laboratory, Oak Ridge, Tennessee 37831-6475, USA*

[5]*Department of Applied Quantum Physics, Kyushu University, Fukuoka 812-0395, Japan*

[6]*Brockhouse Institute for Materials Research, McMaster University, Hamilton, Ontario, Canada L8S 4M1*

[7]*Canadian Institute for Advanced Research, 180 Dundas Street West, Toronto, Ontario, Canada M5G 1Z8*

(Received 1 July 2011; revised manuscript received 11 August 2011; published 22 September 2011)

$CuMoO_4$ is a triclinic quantum magnet based on $S = 1/2$ moments at the Cu^{2+} site. It has recently attracted interest due to the remarkable changes in its chromic and volumetric properties at high temperatures and in its magnetic properties at low temperatures. This material exhibits a first-order structural phase transition at $T_C \sim 190$ K as well as a magnetic phase transition at $T_N \sim 1.75$ K. We report low-temperature heat capacity measurements as well as extensive elastic and inelastic neutron scattering measurements on powder samples taken above and below T_N. We observe neutron diffraction consistent with a simple (1/2, 0, 0) antiferromagnetic structure indicating a doubling of the a-axis periodicity below T_N. In addition, inelastic neutron scattering above a spin gap of ~2.3 meV is consistent with triplet excitations out of paired $S = 1/2$ moments which form singlet dimers. Low-lying spin wave excitations are also observed and these originate from ordered $S = 1/2$ moments below T_N. Taken together these measurements show the ground state of $CuMoO_4$ to display both nonmagnetic singlets and ferromagnetically coupled spins coexisting within an antiferromagnetic structure below $T_N \sim 1.75$ K.

DOI: 10.1103/PhysRevB.84.094436 PACS number(s): 75.25.−j, 75.10.Jm, 75.40.Cx, 75.40.Gb

I. INTRODUCTION

Quantum magnets, based on $S = 1/2$ local moments, have been of intense recent interest due to the nature of the exotic ground states they display and their relation to high-temperature superconductivity.[1] The ground states they can display are varied. One limiting case is that of a nonmagnetic singlet state typical of quasi-one-dimensional spin-Peierls systems, MEM-$(TCNQ)_2$,[2] $CuGeO_3$,[3,4] TiOCl,[5–7] and TiOBr,[8,9] as well as certain quasi-two-dimensional Shastry-Sutherland systems, such as $Sr_2Cu(BO_3)_2$.[10] However, antiferromagnetic Néel ground states also exist, as occurs in the parent compounds of the high-temperature superconductors, such as La_2CuO_4.[11–13]

$CuMoO_4$ is a triclinic magnetic insulator made up of networks of quantum $S = 1/2$ magnetic moments residing at the Cu^{2+} site.[14,15] Several different polymorphs of $CuMoO_4$ have been reported.[16–20] At high pressure, $CuMoO_4$ crystallizes in two distorted wolframite-like structures, $CuMoO_4$-II and $CuMoO_4$-III, that both display antiferromagnetic order at low temperatures.[21,22] Another polymorph, ϵ-$CuMoO_4$, has a monoclinic crystal structure under ambient conditions and orders magnetically with a ferromagnetic component below ~10 K.[23]

The $CuMoO_4$ polymorphs which are the subject of the present article exhibit two triclinic phases at high and low temperatures and ambient pressure, the α and γ phases, respectively. There is a strongly hysteretic first-order structural phase transition between these two structures at T_C ~190–250 K.[15,16,24] While both the α (high temperature) and γ (low temperature) phases are triclinic, they differ in unit cell volume by a remarkable 13% on either side of T_C, with the low-temperature γ phase displaying the smaller cell volume. This phase change is accompanied by a change in color of the material from green (α) to reddish brown (γ). For this reason, this material is referred to as displaying piezo or thermal chromism, and is of considerable current interest for these properties alone.[25–27]

The lattice parameters for $CuMoO_4$ in both its high temperature (α) phase and its low temperature (γ) phase are listed in Table I as taken from Ref. 15. Along with the unit cell volume reduction of 13% on cooling through T_C, the lattice constant shrinks by ~7%, with the largest change being along the b axis.[15,16,24]

The structure within the α phase can be described in terms of relatively isolated clusters of six Cu-O polyhedra, while within the γ phase the Cu-O polyhedra take on a one-dimensional connectivity within the a-b plane.[14] The connectivity of the CuO_6 octahedra in its γ phase gives rise to chains of "molecules" formed by six corner- and edge-sharing CuO_6 octahedra. Cu^{2+} $S = 1/2$ magnetic moments connected by corner-sharing octahedra are expected to interact via relatively strong antiferromagnetic exchange, due to the ~180° Cu-O-Cu bond angles, while those which are connected by edge-sharing octahedra would experience relatively weaker magnetic coupling. The expectation arising from the connectivity within the six CuO_6 octahedra is that the six $S = 1/2$ moments would form two loosely coupled singlet dimers and two relatively free $S = 1/2$ moments per unit cell at low temperature.[14] This scenario is also supported by new high field magnetization

TABLE I. Lattice parameters for $CuMoO_4$ in its high temperature (α) and its low temperature (γ) phases.[15]

α-$CuMoO_4$ High temperature phase	γ-$CuMoO_4$ Low temperature phase
Space group: $P\bar{1}$ (No. 2)	Space group: $P\bar{1}$ (No. 2)
$a = 9.901(3)$ Å	$a = 9.699(9)$ Å
$b = 6.786(2)$ Å	$b = 6.299(6)$ Å
$c = 8.369(3)$ Å	$c = 7.966(7)$ Å
$\alpha = 101.13(1)^\circ$	$\alpha = 94.62(4)^\circ$
$\beta = 96.88(1)^\circ$	$\beta = 103.36(4)^\circ$
$\gamma = 107.01(1)^\circ$	$\gamma = 103.17(4)^\circ$

measurements which show a magnetization plateau near 1/3 of the saturation magnetization. The form of this magnetization can be modeled with two of six spins within the "molecules" become polarized at low fields and giving rise to the ~1/3 plateau, while the remaining four $S = 1/2$ moments are tied up in nonmagnetic singlets until relatively high fields.[28] The present paper reports on new heat capacity and neutron scattering measurements on polycrystalline $CuMoO_4$ which characterize its magnetic properties above and below $T_N \sim 1.75$ K, within its γ phase structure. As we discuss, the scenario of moments arranged into two loosely coupled singlet dimers and two relatively free $S = 1/2$ moments per unit cell is fully consistent with the measurements we present.

II. EXPERIMENTAL DETAILS

Polycrystalline samples were prepared by mixing the following powders in stoichiometric proportions:

$$MoO_3 + CuO \rightarrow CuMoO_4.$$

The mixed powders were pressed hydrostatically at 65 MPa and annealed in air at 700 °C for 72 h. Powder x-ray diffraction measurements of the final samples revealed high-quality polycrystalline material with very little CuO residue.

In order to investigate the magnetic structure and magnetic excitations associated with the low temperature ground state of $CuMoO_4$, we carried out both elastic and inelastic neutron scattering measurements on polycrystalline samples as a function of temperature and magnetic field on the C2 powder diffractometer and the C5 triple-axis spectrometer at the Canadian Neutron Beam Centre (CNBC), Chalk River, as well as inelastic time-of-flight neutron scattering measurements using the Cold Neutron Chopper Spectrometer (CNCS)[21] at the Spallation Neutron Source (SNS) at Oak Ridge National Laboratory (ORNL).

The polycrystalline samples used for the measurements at CNBC were loaded in a sealed Al can in a ^{4}He exchange gas and mounted in different cryostats: either a pumped ^{3}He or ^{4}He cryostat, in order to achieve temperatures as low as 0.3 K and 1.5 K, respectively, and with magnetic field capabilities up to 7.5 T. For the triple-axis measurements at CNBC, we employed a vertically focusing pyrolytic graphite (PG) monochromator and a flat analyzer with a fixed final energy of $E_f = 14.7$ meV. Two PG filters were used in the scattered neutron beam in order to eliminate higher-order wavelength contamination. A liquid-N_2-cooled sapphire filter was used in the main beam to minimize the fast neutron background. Soller slits in the four beam paths (from source to detector) produced a collimation of [none, 0.48°, 0.56°, 1.2°], resulting in an energy resolution of ~1 meV for these triple-axis measurements.

Time-of-flight neutron scattering measurements were performed using the CNCS at the SNS at ORNL. CNCS is a direct geometry, multichopper inelastic spectrometer optimized for high Q and good E resolution measurements using low incident neutron energies ($E_i < 30$ meV). Measurements were carried out on a 17 g polycrystalline $CuMoO_4$ sample that was loaded in a standard aluminum sample can. The sample environment consisted of a 5 T vertical field magnet cryostat with a base temperature of 1.5 K. A cadmium mask was attached to the sample can to reduce multiple scattering and scattering from the cryostat. The sample was measured using two different settings for the incident neutron energy to cover a broad range of (Q,E) space. $E_i = 6.6$ meV and $E_i = 1.55$ meV were employed for moderate and high energy resolution measurements, respectively. For all measurements, the spectrometer was run in the high-flux configuration and the double-disk chopper was phased at 180 Hz, providing elastic energy resolutions of ~0.18 and ~0.025 meV for the two E_i settings, respectively.

III. HEAT CAPACITY MEASUREMENTS

We carried out heat capacity measurements at low temperatures to characterize the magnetic phase behavior in $CuMoO_4$. Figure 1 shows heat capacity measurements as a function of temperature and magnetic field, up to 4 T. The measurements were performed using the quasi-adiabatic heat pulse method and a ^{3}He refrigerator. The heat capacity measurements at $H = 0$ T reveal a λ-like anomaly signifying a magnetic phase transition at $T_N \sim 1.75$ K, as well as a weaker peak near ~2.2 K, likely indicating a buildup of short range

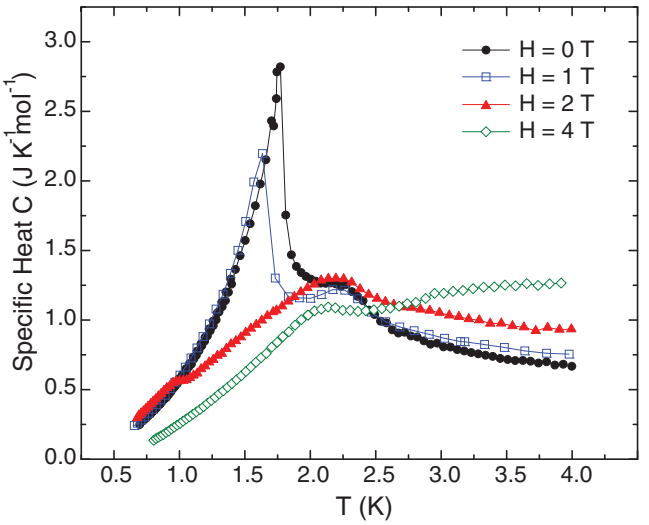

FIG. 1. (Color online) The temperature dependence of the heat capacity of $CuMoO_4$ as observed in zero magnetic field as well as in magnetic fields up to 4 T.

correlations at that temperature. The sharp λ-like anomaly moves to lower temperatures and weakens in amplitude on application of a magnetic field. The transition appears to have been fully suppressed for fields >2 T, with only a broad anomaly remaining in the heat capacity at ∼2.2 K for higher fields.

IV. NEUTRON SCATTERING RESULTS AND DISCUSSION

We performed two sets of neutron powder diffraction measurements on $CuMoO_4$. The first of these, shown in Fig. 2(a), was performed on the C2 powder diffractometer at CNBC, Chalk River, using an incident neutron wavelength of $\lambda = 2.37$ Å. Figure 2(a) shows the relatively low angle portion of the neutron diffraction pattern at $T = 5$ K and $T = 0.4$ K. The neutron intensity is plotted on a log scale, and a clear temperature-dependent, resolution-limited Bragg peak is observed at a scattering angle of ∼7.4° for which $Q = 0.34$ Å^{-1}. Two additional, much weaker features are seen in the difference between the $T = 0.4$ K and $T = 5$ K data sets near $Q = 1.04$ and 1.26 Å^{-1}. These three peaks were the only additional Bragg peaks to appear on cooling through $T_N \sim 1.75$ K.

Powder diffraction measurements were also performed on the C5 triple-axis spectrometer which allowed a parametric study of the temperature and magnetic field dependence of the low temperature Bragg peak at $Q = 0.34$ Å^{-1} shown in Fig. 2(a). These order parameter measurements are shown in Figs. 3(a) and 3(b) for the temperature dependence at zero field and the field dependence at $T = 0.4$ K, respectively. This field and temperature dependence of the order parameter identify the new low temperature Bragg peak as magnetic in origin and corresponding to the sharp anomaly observed in the zero-field heat capacity, as shown in Fig. 1. Interestingly, the phase transition appears to be continuous as a function of temperature at zero field [Fig. 3(a)] but rather discontinuous as a function of field at low temperatures [Fig. 3(b)].

While we have observed only three magnetic Bragg peaks for $CuMoO_4$ below T_N, we can model its magnetic structure, based on its periodicity as shown in Fig. 2(b), wherein we pair off four of the six $S = 1/2$ moments per unit cell into two singlets, and allow the remaining two spins to order ferromagnetically within a unit cell and to order antiferromagnetically from cell to cell along the triclinic a direction. The rationale for pairing four of the six $S = 1/2$ spins per unit cell off into nonmagnetic singlets comes both from recent high field magnetization studies[28] and from inelastic neutron scattering results which we report below. The magnitude of the ordering wave vector associated with the strong magnetic Bragg peak at $Q = 0.34$ Å^{-1} is correctly accounted for by the magnitude of the resulting (1/2, 0, 0) antiferromagnetic ordering wave vector within this triclinic structure. This tells us that the magnetic unit cell is doubled along the a direction, relative to the chemical structure. We can calculate the magnetic Bragg scattering for two cases, Models I and II, where the two spins couple ferromagnetically within a unit cell and antiferromagnetically from cell to cell along a [shown in Fig. 2(b)] and the case where they couple antiferromagnetically both within a unit cell and from unit cell to unit cell along a,

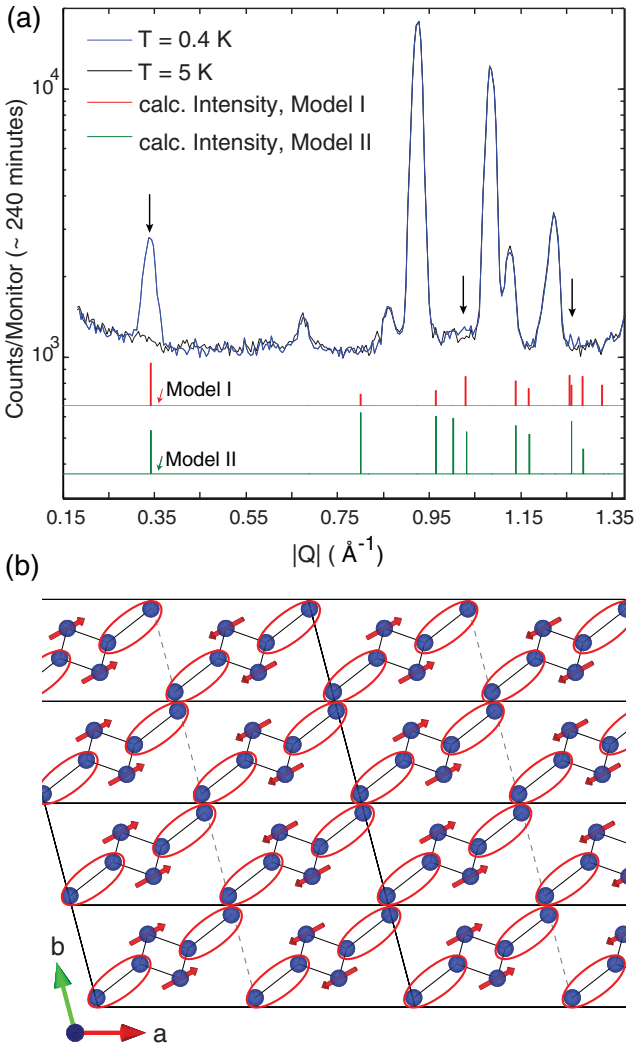

FIG. 2. (Color online) (a) Powder neutron diffraction measured at the C2 powder diffractometer at CNBC showing the magnetic Bragg peaks (indicated by arrows) at $|Q| \sim 0.34$ Å^{-1}, $|Q| \sim 1.03$ Å^{-1}, and $|Q| \sim 1.26$ Å^{-1} at ∼0.4 K. A complete powder diffraction pattern using the position-sensitive linear detector took ∼240 min to acquire. The calculated intensity $I(|Q|)$ (in arbitrary units) of the magnetic Bragg scattering based on the two models discussed in the text is shown on a log scale and has been offset along the y axis for clarity. (b) The proposed spin configuration in the $H = 0$ T ground state of $CuMoO_4$, based on ferromagnetically coupled spins within a unit cell, which order antiferromagnetically along a, consistent with the (1/2, 0, 0) ordering wave vector. Black solid lines depict the magnetic unit cell, which is doubled along the a axis relative to the chemical unit cell (dashed gray lines). The direction of the moments within the unit cell has been derived from the best fit to Model I, which correctly accounts for the observed powder diffraction pattern shown in panel (a). Inelastic scattering indicates the presence of triplet excitations out of paired singlets, shown as ellipses surrounding the $S = 1/2$ moments, which pair to form the singlets and which participate in the magnetic structure.

respectively. These calculated magnetic Bragg intensities are shown in Fig. 2(a), also on a log intensity scale, along with the measured powder neutron diffraction at $T = 0.4$ K and

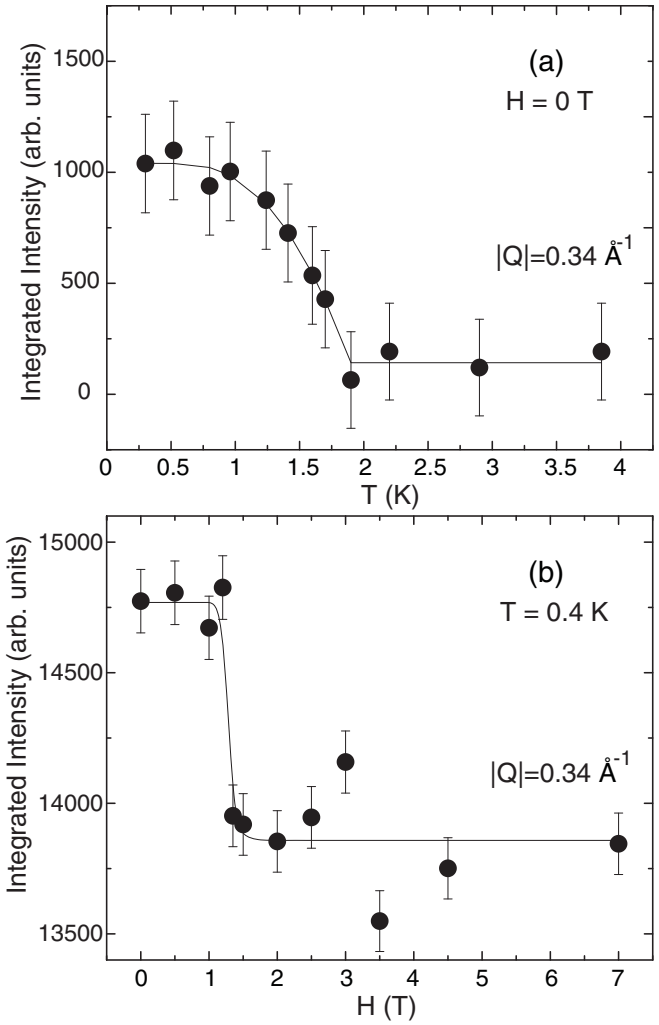

FIG. 3. (a) The antiferromagnetic order parameter as measured by the integrated intensity of the $Q = 0.34$ Å^{-1} Bragg peak is shown as a function of temperature. A high-temperature ($T = 50$ K) background has been subtracted from this data set. (b) The same antiferromagnetic Bragg intensity at $Q = 0.34$ Å^{-1} is shown as a function of magnetic field at $T \sim 0.4$ K, within the magnetically ordered state. While the thermal evolution of the transition appears continuous in zero field, the antiferromagnetic order drops discontinuously to zero with field at low temperatures. The lines in both (a) and (b) are guides to the eye, with error bars of σ from counting statistics. Both data sets shown are obtained on the triple-axis spectrometer C5 at the CNBC.

$T = 5$ K. The best descriptor of the powder diffraction data is for Model I, where the two "free" spins within a unit cell (those not involved in the singlets) point approximately along the diagonal of the unit cell, along the interdimer bond direction. These $S = 1/2$ moments align ferromagnetically within a unit cell and antiferromagnetically from cell to cell along a, as shown in Fig. 2(b).

The inelastic data sets are consistent with low energy spin wave excitations in the ordered state below T_N [Fig. 4(a)] coexisting with a gapped excitation spectrum characteristic of triplet excitations out of a singlet ground state. The triplet excitations have a bandwidth of ~2.5 meV, with a gap of ~2.3 meV. The band width likely originates from weak dispersion within the triplet of excited states due to interdimer

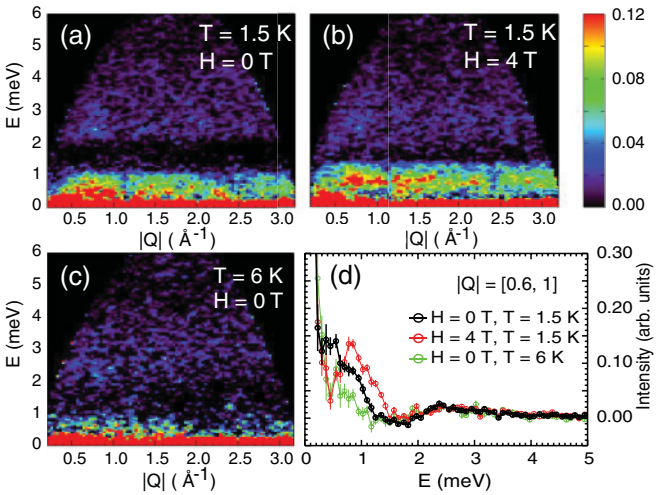

FIG. 4. (Color online) Color contour maps of $S(Q,E)$ observed in $CuMoO_4$ are shown for $E_i = 6.6$ meV at $T = 1.5$ K in zero applied magnetic field (a) and in an $H = 4$ T magnetic field (b). Panel (c) shows $S(Q,E)$ in the $H = 0$ T paramagnetic phase at $T = 6$ K. An energy cut through $S(Q,E)$ for an interval of $|Q| = 0.6$ to 1 Å^{-1}. A high-temperature background (at $T = 50$ K, within the paramagnetic state) has been subtracted from all panels to isolate the magnetic scattering.

exchange coupling, as observed in other singlet ground state systems such as $SrCu_2(BO_3)_2$.[10]

We also carried out two sets of inelastic neutron scattering measurements on this polycrystalline sample. We will first describe time-of-flight inelastic measurements taken with the CNCS chopper spectrometer at SNS and then triple-axis measurements taken with the C5 spectrometer at CNBC, Chalk River.

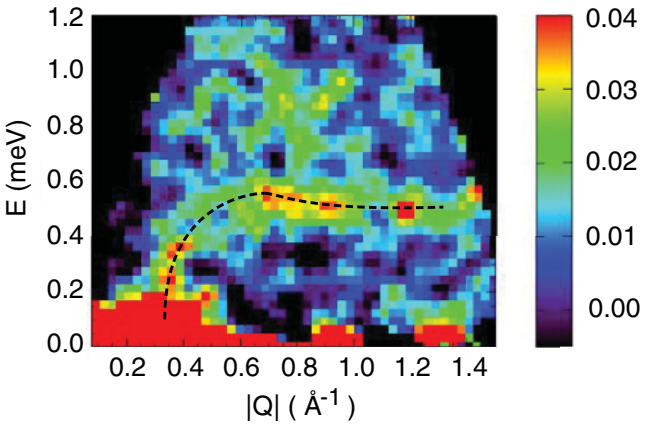

FIG. 5. (Color online) A high energy resolution measurement of S(Q, E) using CNCS and an incident neutron energy of $E_i = 1.55$ meV is shown for $CuMoO_4$ at $T = 1.5$ K and $H = 0$ T. A high temperature ($T = 50$ K) background data set has been subtracted from the data set. The low energy spin dynamics are seen to consist of a Goldstone mode emanating from the ordering wave vector, $Q = 0.34$ Å^{-1}, and a relatively dispersionless band of excitations near 0.5 meV. Magnetic spectral weight is observed out to ~1 meV.

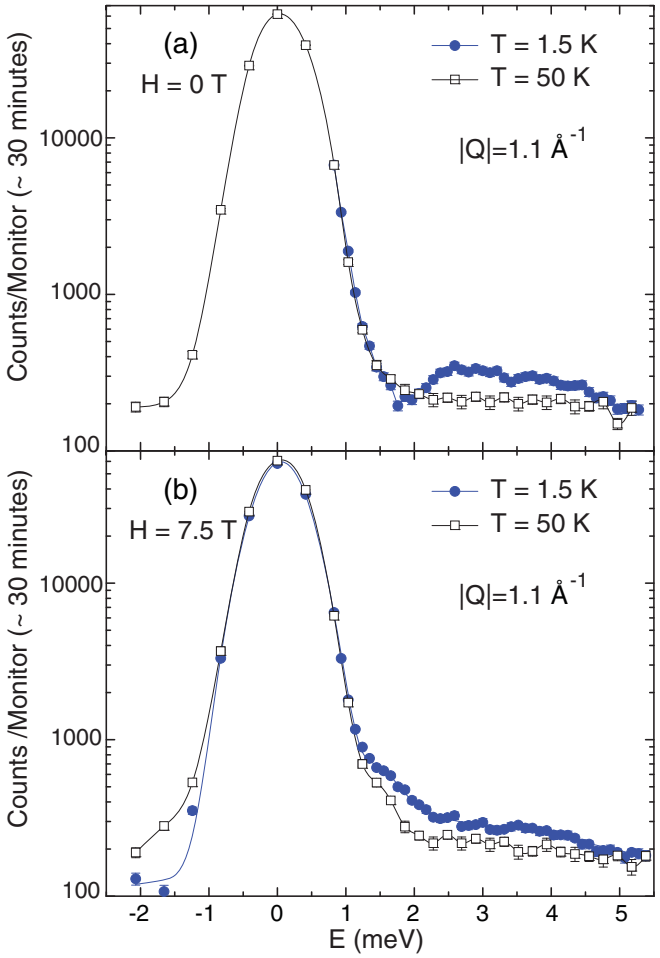

FIG. 6. (Color online) (a) Relatively low energy resolution inelastic scattering at $Q = 1.1$ Å^{-1} reveals a gapped spin excitation spectrum in the ordered state at $T = 1.5$ K and in zero magnetic field. The gap is ~2.3 meV with a bandwidth of ~2.5 meV. (b) At the largest applied magnetic field, we observe the lower bound of the zero-field triplet band to extend well within the ~2.3 meV gap. Note the logarithmic intensity scale.

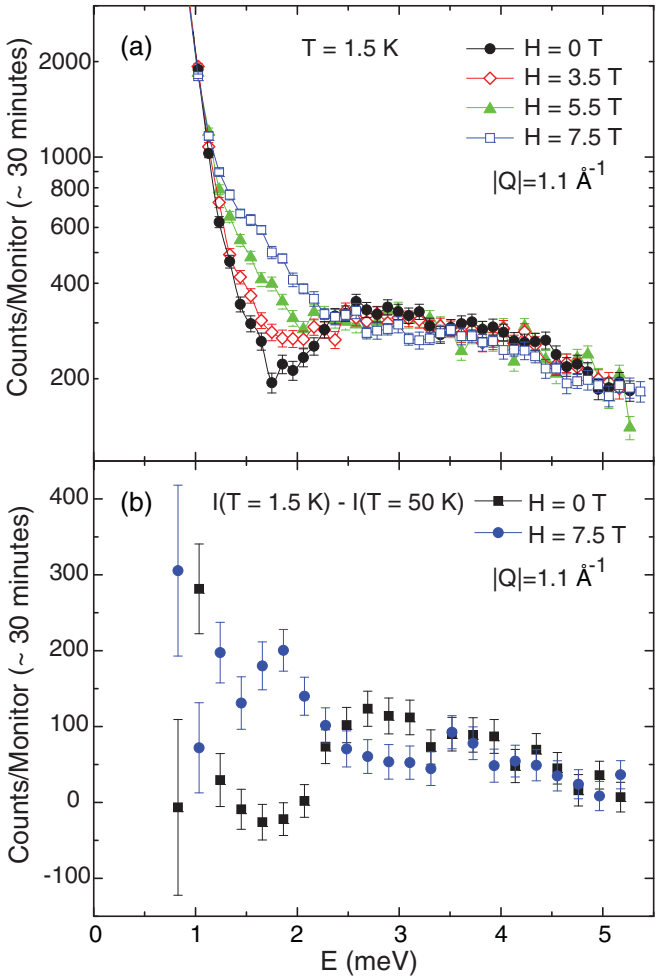

FIG. 7. (Color online) (a) The effect of application of a magnetic field in the range of 0 to 7.5 T on the magnetic excitation spectrum is shown in $CuMoO_4$. (b) The high-temperature background-subtracted inelastic intensity at zero field and at an applied field of 7.5 T is shown. Clearly, the bottom of the triplet scattering near ~2.5 meV is depleted and transferred down to ~1.75 meV, within the gap, by application of the magnetic field. This is consistent with expectations for Zeeman splitting of a weakly dispersive triplet band. Simultaneously, the spectral weight of the low energy spin wave excitations are moved to higher energies within the gap. Note that the intensity scale is logarithmic in (a) and linear in (b).

The inelastic excitation spectrum for $CuMoO_4$ is shown in Fig. 4 as a color contour map of the inelastic neutron scattering intensity, $S(Q,E)$, for an incident neutron energy of $E_i = 6.6$ meV. Figures 4(a), 4(b), and 4(c) show this spectrum in the ordered phase below T_N at $T = 1.5$ K and at zero applied magnetic field; in the disordered phase at base temperature $T = 1.5$ K and $H = 4$ T; and in the paramagnetic phase at $H = 0$ T and $T = 6$ K, respectively. Figure 4(d) shows a cut in energy, of these same three data sets, integrated in Q for $|Q| = [0.6,1.0]$ Å^{-1}. These data sets have had a high temperature, 50 K, $H = 0$ T background data set subtracted from them.

On applying an $H = 4$ T magnetic field at low temperatures [Fig. 4 (b)], the bottom of the triplet band moves down to below ~1.9 meV, consistent with an expected downward shift of the energy of the lowest of the three triplet states by $\Delta E = g\mu_B H = 0.46$ meV for $g = 2$ and $H = 4$ T. The low-energy spin wave scattering is also raised in energy, and the spin wave spectrum appears to be gapped. This can be seen more clearly in the energy cuts of this same data shown in Fig. 4(d), wherein a $H = 4$ T magnetic field appears to deplete the low energy spectrum below ~0.5 meV for $T = 1.5$ K and $H = 0$ T, and it induces a pronounced inelastic peak at ~0.8 meV.

Higher energy resolution measurements were also taken with CNCS using an incident neutron energy of $E_i = 1.55$ meV, and these are shown for $T = 1.5$ K in Fig. 5. Again a high-temperature data set at $T = 50$ K and $H = 0$ T has been subtracted from this data set to isolate the magnetic scattering from the sample. This higher energy resolution data set clearly shows a Goldstone spin wave mode emanating out of the magnetic Bragg peak position at $Q = 0.34$ Å^{-1}. Beyond ~ 0.6 Å^{-1} the spin wave density of states is strongly peaked at ~0.55 meV; however, a second distribution of magnetic scattering, with a bandwidth of ~0.25 meV is evident between 0.7 and 1.0 meV. These two bands of spin wave scattering account for the quasi-elastic magnetic scattering observed

with lower energy resolution (Fig. 4) wherein quasi-elastic scattering is observed out to ∼1 meV. Given that the magnetically ordered ground state below T_N is described by an antiferromagnetic alternation of ferromagnetically coupled spins along the trigonal a direction, it is not surprising that two bands of spin wave excitations, an acoustic and an optic band, would be present at low temperatures.

Constant-$Q = 1.1$ Å^{-1} inelastic neutron scattering measurements carried out with the C5 triple axis spectrometer at CNBC, Chalk River, are shown in Figs. 6 and 7. These largely corroborate the time-of-flight measurements show in Figs. 4 and 5, although they are carried out to larger applied magnetic fields, up to $H = 7.5$ T. These measurements were performed with an energy resolution of ∼1 meV, and thus detail within the quasi-elastic spin wave band of scattering is obscured by nuclear elastic incoherent scattering. Nonetheless, the triplet excitations and singlet-triplet gap can be clearly observed, as well as the filling of the gap with increasing magnetic field.

Figure 6(a) shows $S(Q = 1.1$ Å$^{-1}, E)$ for $T = 1.5$ K and $T = 50$ K and zero magnetic field, while Fig. 6(b) shows the same spectra but for $H = 7.5$ T. Figure 7(a) shows the field dependence of $S(Q = 1.1$ Å$^{-1}, E)$ at $T = 1.5$ K, while Fig. 7(b) focuses on the low energy part of this spectrum, for $H = 0$ T and $H = 7.5$ T only, after the high-temperature background at $T = 50$ K has been subtracted from both data sets. Note that the intensity scale for Figs. 6(a), 6(b), and 7(a) is logarithmic, while that of Fig. 7(b) is linear. This comparison clearly shows spectral weight from the low energy side of the triplet band being depleted and displaced downward in energy by $g\mu_B H \sim 0.7$ meV to ∼1.6 meV, consistent with the expected Zeeman splitting of the lowest energy state within the triplet. The low-energy spin waves are also raised in energy by application of a field, and this also pushes magnetic intensity into the gap. The higher end of the triplet bandwidth, above 3.5 meV, shows less field dependence, but the scattering is weaker here. This relative lack of field dependence at mid-triplet band energies (∼3.5 meV) and higher is likely a consequence of the S^z mode of the triplet, for which there is no Zeeman effect, and the averaging effects of the triplet dispersion.

V. CONCLUSIONS

We have carried out heat capacity and both elastic and inelastic neutron scattering measurements on powder samples of the triclinic quantum magnet $CuMoO_4$ with the purpose of understanding the nature of its low temperature ground state. All results are consistent with an antiferromagnetic long range ordered ground state appearing below $T_N = 1.75$ K in $H = 0$ T. The ordering wave vector associated with this antiferromagnetic order is identified as (1/2, 0, 0), and this is consistent with a low-temperature state in which the molecule of six Cu^{2+} ions, which makes up the triclinic structure, organizes into four $S = 1/2$ moments which form two singlets, as well as two ferromagnetically coupled $S = 1/2$ moments which then order antiferromagnetically along the triclinic a direction. We explicitly show that at low temperatures this ordered state is destroyed by an applied magnetic field of ∼1.5 T.

Our inelastic neutron scattering measurements on $CuMoO_4$ probe the magnetic excitation spectrum and show it to be well described by dispersive triplet excitations with a gap of ∼2.3 meV and a bandwidth of ∼2.5 meV. Low-lying spin wave excitations are also observed and are shown to display a Goldstone mode for $T < T_N$, which is soft at the ordering wave vector of $Q \sim 0.34$ Å^{-1}, as well as a second branch of spin wave excitations forming a band in the approximate range 0.6–1.0 meV.

The picture arising from the measurements we present, of an antiferromagnetic long range ordered structure made up of coexisting nonmagnetic singlets and ferromagnetically coupled spins, is clearly exotic, composed as it is by both of the ground states normally associated with antiferromagnetism in materials. $CuMoO_4$ is clearly an interesting and exotic example where both ordered spins and singlets are the building blocks from which the antiferromagnetic ground state is constructed. We hope this study will guide and inform further theoretical studies of this and related quantum magnets.

ACKNOWLEDGMENTS

We wish to acknowledge the contributions of K. A. Ross and J. P. C. Ruff to the neutron scattering measurements reported here. This work was supported by NSERC of Canada and by the Research Exchange Program between JSPS and NSERC and Grants-in-Aid for Scientific Research, MEXT (Grant No. 21560723).

*Current affiliation: The Advanced Photon Source, Argonne National Laboratory, Argonne, Illinois 60439, USA, and The James Franck Institute and Department of Physics, The University of Chicago, Chicago, Illinois 60637, USA.

[1]See, for example, E. Dagotta and T. M. Rice, Science **271**, 618 (1996); and A. T. Skjeltorp and D. Sherrington (editors), *Dynamical Properties of Unconventional Magnetic Systems*, NATO ASI, Series E, Vol. 348 (Kluwer Academic, Boston, 1998).

[2]M. D. Lumsden and B. D. Gaulin, Phys. Rev. B **59**, 9372 (1999), and references contained therein.

[3]M. Hase, I. Terasaki, and K. Uchinokura, Phys. Rev. Lett. **70**, 3651 (1993).

[4]J. P. Pouget, L. P. Regnault, M. Ain, B. Hennion, J. P. Renard, P. Veillet, G. Dhalenne, and A. Revcolevschi, Phys. Rev. Lett. **72**, 4037 (1994).

[5]T. Imai and F. C. Chou, e-print arXiv:cond-mat/0301425.

[6]S. R. Saha, S. Golin, T. Imai, and F. C. Chou, J. Phys. Chem Solids **68**, 2044 (2007).

[7]J. P. Clancy, B. D. Gaulin, J. P. Castellan, K. C. Rule, and F. C. Chou, Phys. Rev. B **78**, 014433 (2008).

[8] J. P. Clancy, B. D. Gaulin, and F. C. Chou, Phys. Rev. B **81**, 024411 (2010).
[9] J. P. Clancy, B. D. Gaulin, C. P. Adams, G. E. Granroth, A. I. Kolesnikov, T. E. Sherline, and F. C. Chou, Phys. Rev. Lett. **106**, 117401 (2011).
[10] B. D. Gaulin, S. H. Lee, S. Haravifard, J. P. Castellan, A. J. Berlinsky, H. A. Dabkowska, Y. Qiu, and J. R. D. Copley, Phys. Rev. Lett. **93**, 267202 (2004).
[11] D. Vaknin, S. K. Sinha, D. E. Moncton, D. C. Johnston, J. M. Newsam, C. R. Safinya, and H. E. King, Jr., Phys. Rev. Lett. **58**, 2802 (1987).
[12] G. Shirane, Y. Endoh, R. J. Birgeneau, M. A. Kastner, Y. Hidaka, M. Oda, M. Suzuki, and T. Murakami, Phys. Rev. Lett. **59**, 1613 (1987).
[13] M. A. Kastner, R. J. Birgeneau, G. Shirane, and Y. Endoh, Rev. Mod. Phys. **70**, 897 (1998).
[14] T. Ito, H. Takagi, and T. Asano, Chem. Mater. **21**, 3376 (2009).
[15] M. Wiesmann, H. Ehrenberg, G. Miehe, T. Peun, H. Weitzel, and H. Fuess, J. Solid State Chem. **132**, 88 (1997).
[16] H. Ehrenberg, H. Weitzel, H. Paulus, M. Wiesmann, G. Wltschek, M. Geselle, and H. Fuess, J. Phys. Chem. Solids **58**, 153 (1997).
[17] S. C. Abrahams, J. L. Bernstein, and P. B. Jamieson, J. Chem. Phys. **48**, 2619 (1968).
[18] A. W. Sleight, Mater. Res. Bull. **8**, 863 (1973).
[19] R. Kohlmuller and J.-P. Faurie, Chim. Mineral.- Acad. Sci. C **264**, 1751 (1967).
[20] R. Kohlmuller and J.-P. Faurie, Bull. Soc. Chim. Fr. **1968**, 4379 (1968).
[21] H. Ehrenberg, M. Wiesmann, J. Garcia-Jaca, H. Weitzel, and H. Fuess, J. Magn. Magn. Mater. **182**, 152 (1998).
[22] H.-J. Koo and M.-H. Whangbo, Inorg. Chem. **40**, 2161 (2001).
[23] J. Baek, A. S. Sefat, D. Mandrus, and P. S. Halasyamani, Chem. Mater. **20**, 3786 (2008).
[24] F. Rodríguez, D. Hernández, J. Garcia-Jaca, H. Ehrenberg, and H. Weitzel, Phys. Rev. B **61**, 16497 (2000).
[25] M. Gaudon, P. Deniard, A. Demourgues, A.-E. Thiry, C. Carbonera, A. Le Nestour, A. Largeteau, J.-F. Létard, and S. Jobic, Adv. Mater. **20**, 3517 (2007).
[26] G. Steiner, R. Salzer, and W. Reichelt, Fresenius' J. Anal. Chem. **370**, 731 (2000).
[27] A.-E. Thiry, M. Gaudon, C. Payen, N. Daro, J.-F. Létard, S. Gorsse, P. Deniard, X. Rocquefelte, A. Demourgues, M.-H. Whangbo, and S. Jobic, Chem. Mater. **20**, 2075 (2008).
[28] T. Asano, T. Nishimura, S. Ichimura, Y. Inagaki, T. Kawae, T. Fukui, Y. Narumi, K. Kindo, T. Ito, S. Haravifard, and B. D. Gaulin, J. Phys. Soc. Jpn. **80**, 093708 (2011).
[29] T. E. Mason, D. Abernathy, I. Anderson, J. Ankner, T. Egami, G. Ehlers, A. Ekkebus, G. Granroth, M. Hagen, K. Herwig, J. Hodges, C. Hoffmann, C. Horak, L. Horton, F. Klose, J. Larese, A. Mesecar, D. Myles, J. Neuefeind, M. Ohl, C. Tulk, X. L. Wang, and J. Zhao, Physica B **385-386**, 955 (2006).